Desalination and Water Treatment
www.deswater.com

doi: 10.1080/19443994.2015.1033648

57 (2016) 10604–10615
May

Taylor & Francis
Taylor & Francis Group

Preparation of a cellulose-based adsorbent with covalently attached hydroxypropyldodecyldimethylammonium groups for the removal of C.I. Reactive Blue 21 dye from aqueous solution

Dongying Hu, Peng Wang, Qianyun Ma, Lijuan Wang*

Key Laboratory of Bio-based Material Science and Technology of Ministry of Education, Northeast Forestry University, 26 Hexing Road, Harbin 150040, P.R. China, Tel. +86 451 82191693; emails: 465257973@qq.com (D. Hu), 121940994@qq.com (P. Wang), 1477293457@qq.com (Q. Ma), Tel./Fax: +86 451 82191693; email: donglinwlj@163.com (L. Wang)

Received 12 August 2014; Accepted 20 March 2015

ABSTRACT

An adsorbent for the removal of C.I. Reactive Blue 21 (RB21) dye from aqueous solution was prepared by covalently attaching hydroxypropyldodecyldimethylammonium groups to microcrystalline cellulose. The adsorbent was characterized using FTIR, ^{13}C NMR spectroscopy, and SEM. Adsorption studies were conducted to evaluate the effects of adsorbent loading, contact time, dye concentration, pH, temperature, and ionic strength. Adsorption kinetics and isotherms were fitted to different models. FTIR and ^{13}C NMR studies indicated that the quaternary ammonium group had been successfully attached to the cellulose. SEM photographs showed that the surface became coarser after the modification. The cellulose-based adsorbent was shown to be very efficient for the removal of RB21 dye, with equilibrium being reached in 180 min. Maximum adsorption of RB21 dye was achieved at pH 2. The adsorption of RB21 dye onto the adsorbent was a spontaneous endothermic process and satisfactorily fitted the pseudo-second-order kinetic model, the intraparticle diffusion model, and the Langmuir adsorption isotherm model. An adsorption capacity of 200 mg/g was achieved, indicating an excellent adsorption performance.

Keywords: Microcrystalline cellulose; Modification; Quaternary ammonium group; Adsorption; C.I. Reactive Blue 21; Kinetics; Isotherms; Thermodynamics

1. Introduction

In recent years, environmental pollution—especially that caused by dyes in wastewater—has attracted increasing attention from the international community [1]. Dyes can be divided into three categories: cationic dyes (direct, acid, and reactive dyes), anionic dyes (basic dyes), and non-ionic dyes (disperse dyes) [2]. These dyes are widely used in many industrial processes, including production of dyestuffs, paper, leather, cosmetics, and textiles as well as electrophoresis [3]. Discharge of dyes into water courses presents a serious threat to both the natural environment and human health [4], since most dyes are highly toxic, non-biodegradable, carcinogenic, and mutagenic for humans and other living organisms [5]. Reactive dyes are typically azo-based chromophores combined with a reactive group that bonds with the material being dyed. Reactive dyes cannot be removed by conventional wastewater treatment because of their

*Corresponding author.

stability towards light, heat, and oxidizing agents [6]. From an environmental point of view, there is thus an urgent need to find an effective method for the removal of dyes from wastewater.

Many techniques, including coagulation, advanced oxidation, photocatalytic degradation and biological treatment [7,8], have been used for removing dyes from wastewater. The widespread application of these techniques has, however, been impeded by poor efficiency, high cost, or formation of toxic intermediate products. Biosorption is proving to be an effective method for the purification of dye wastewater and many materials, including activated carbon, agricultural waste, industrial waste, biomass, and other polysaccharide materials [9] which have been studied as a biosorbents. Activated carbon, a versatile adsorbent, is effective for the removal of dyes from wastewater but high costs and recycling difficulties have limited its practical application [10]. Many research groups have thus focused on identifying low-cost adsorbents with high adsorption capacities for the decoloration of dye wastewater [11].

Cellulose, which consists of a linear chain of many β (1 → 4) linked D-glucose units, is the most abundant natural polymer on Earth. It is non-toxic, biodegradable, renewable, and sustainable [12]; and can also be chemically modified through reaction of the active hydroxyl groups on the glucose units. Chemically modified cellulose has been used as an adsorbent for heavy metals [13] and dyes [14]. As an example, diethylenetriamine-bacterial cellulose has been used as an adsorbent for the removal of Cu(II) and Pb(II) [15]. The adsorption capacity of cellulose is significantly improved after treatment with amines [16]; modified celluloses have been prepared by treatment with 3-chloro-2-hydroxypropyltriethylammonium chloride [17,18], triethylamine [19], and tetramethylethylenediamine [20]. Cationic modification of cellulose with quaternary ammonium salts is especially effective for treating wastewater containing anionic dyes. To the best of our knowledge, there have been no reports describing attachment of hydroxypropyldodecyldimethylammonium groups to microcrystalline cellulose (MCC) as an adsorbent for the removal of dyes from aqueous solution.

In this work, a highly effective adsorbent based on MCC was prepared by linking hydroxypropyldodecyldimethylammonium groups to the backbone of MCC. The modified MCC (MMCC) was characterized by Fourier transform infrared (FTIR), solid-state cross-polarization magic angle spinning ^{13}C NMR and scanning electron microscopy (SEM). The product was tested as an adsorbent for C.I. Reactive Blue 21 (RB21) dye from aqueous solutions under different conditions. Variables included adsorbent dosage, contact time, dye concentration, temperature, pH, and ionic strength. The kinetics, isotherms, and thermodynamics of the adsorption process were also studied.

2. Experimental

2.1. Materials

MCC was purchased from HengXin Chemical Reagent Co. Ltd. (Shanghai, China). *N*,*N*-dimethyl-1-dodecylamine ($C_{14}H_{31}N$; 98% pure; M.W: 213.4) was obtained from Heowns Chemical Reagent Co. Ltd. (Tianjin, China). Epichlorohydrin was purchased from Kemiou Chemical Reagent Co. Ltd. (Tianjin, China). RB21 (λ_{max} 660 nm), a copper phthalocyanine with a sulfatoethylsulfone reactive group, was supplied by DyStar Trading Co. Ltd. (Shanghai, China). Its molecular structure is shown in Fig. 1. All other chemicals and reagents used in this work were of analytical grade. All solutions were prepared using distilled water.

2.2. Preparation of the adsorbent

A mixture of MCC (10 g) and 20 wt.% NaOH solution (250 mL) was exposed to ultrasonic radiation at a power of 10.8 kJ/g for 5 min and then stirred for 2 h at room temperature. The solvent was removed and the residue was treated immediately with epichlorohydrin (240 mL) and 10 wt.% NaOH solution (250 mL). After stirring at 65°C for 6 h, all the solution was removed immediately from the heat mixture and 40 v/v% *N*,*N*-dimethyldodecylamine in isopropanol (100 mL) was added. The mixture was heated to 80°C and agitated for 3 h. The solvent was then removed and the residue washed thoroughly with anhydrous ethanol, distilled water, 0.1 M NaOH solution, and 0.1 M HCl solution. The MMCC was finally rinsed thoroughly with distilled water and dried *in vacuo* at 60°C for 12 h. Possible reactions involved in this process are shown in Fig. 2.

2.3. Characterization of the adsorbent

FTIR spectra of the MCC and MMCC were obtained using a Nicolet 6700 instrument (Thermo Fisher Scientific Co., Ltd., MA, USA) using attenuated total reflection at a resolution of 4 cm^{-1}. A solid-state CP/MAS ^{13}C NMR spectrum of MMCC was recorded at 291.60 K on a Bruker DRX-400 spectrometer, using a 4 mm diameter zirconia MAS rotor, a MAS rate of

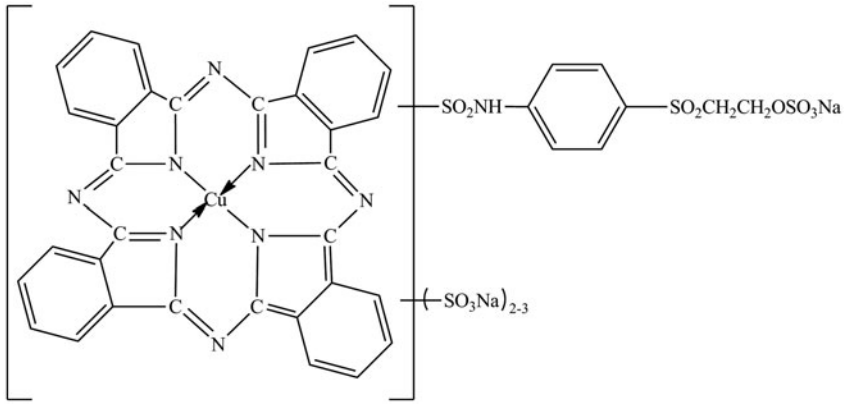

Fig. 1. Molecular structure of RB21 dye.

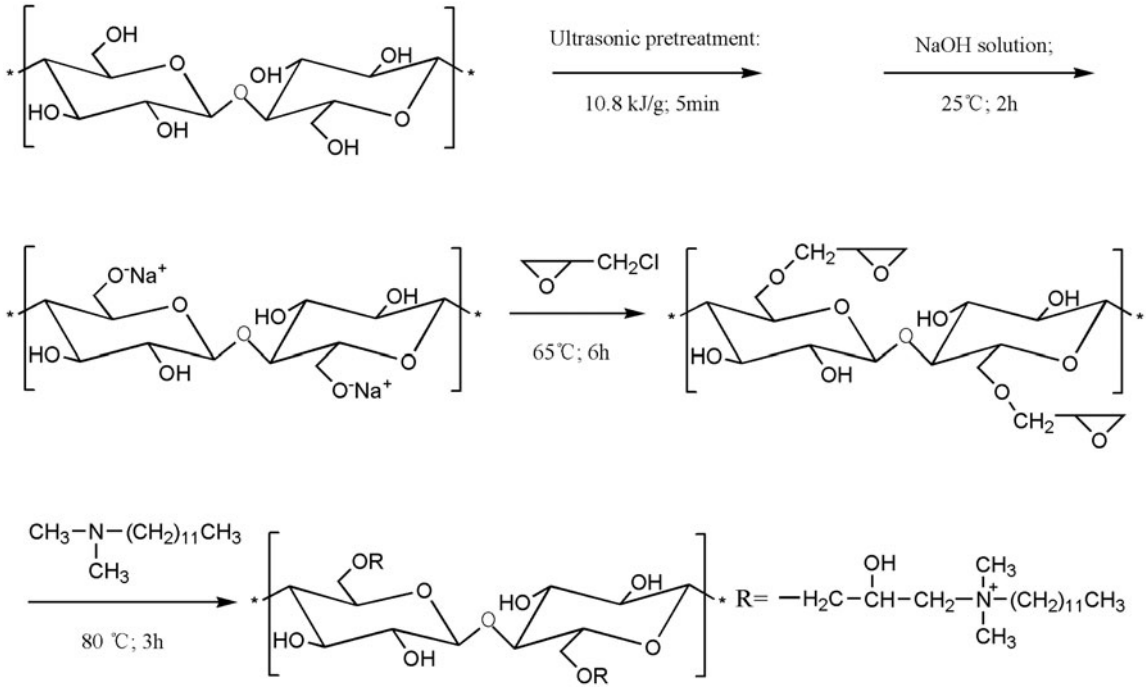

Fig. 2. Synthetic reaction for the MMCC.

5 kHz, a contact time of 1,000 μs, and a frequency of 75.47 MHz. The spectrum was recorded over 19 h. Surface morphological analyses of MCC and MMCC were conducted using a Quanta 200 scanning electron microscope (Philips-FEI Co., AMS, Netherlands). The surfaces of the samples were coated with thin layers of gold before determination. The absorption spectrum of the solution was measured using a UV–visible spectrophotometer (TU-1900, Beijing Purkinje General Instrument Co. Ltd., China). The wavelength of maximum absorption (λ_{max}) for the RB21 dye was 660 nm. The point of zero charge (pH_{pzc}) was determined by the solid addition method [21].

2.4. Adsorption experiments

Adsorption experiments were performed to obtain equilibrium data and evaluate the effects of different factors, including adsorbent dosages, contact time, initial dye concentrations, adsorption temperatures, and pH values. In each experiment, RB21 dye solution (100 mL) was shaken at 120 rpm with a known quantity

of the adsorbent for sufficient time for the adsorption process to reach equilibrium. After the adsorption period, the absorbance of the RB21 dye solution was measured at 660 nm using a UV–visible spectrophotometer, and the equilibrium concentration was calculated using the standard curve equation for the RB21 dye. The dye removal efficiency (R) and the adsorption capacities (q_e and q_t) for RB21 dye can be calculated by the following equations:

$$R = (C_0 - C_t)/C_0 \times 100\% \quad (1)$$

$$q_e = (C_0 - C_e) \times V/M \quad (2)$$

$$q_t = (C_0 - C_t) \times V/M \quad (3)$$

where q_e (mg/g) and q_t (mg/g) are the amounts of adsorbed dye per unit mass of adsorbent at equilibrium and at time t (min), C_0 (mg/L) is the initial dye concentration, C_t is the dye concentration at time t (min), C_e (mg/L) is the equilibrium concentration of the dye solution, V (mL) is the volume of the dye solution, and M (mg) is the amount of MMCC.

2.5. Adsorption kinetics and isotherms

2.5.1. Kinetic models

For the kinetic studies, adsorption experiments were performed by shaking the adsorbent (40 mg) with dye solution (100 mL) at different temperatures (303, 313, and 323 K). Pseudo-first-order and pseudo-second-order models were used for analysis of the adsorption process [22]. The pseudo-first-order model and the pseudo-second-order model are generally used to describe the initial stage of the adsorption process and the entire adsorption process, respectively. The pseudo-first-order model is expressed as:

$$\ln (q_e - q_t) = \ln q_{el} - k_1 t \quad (4)$$

where q_e (mg/g) and q_t (mg/g) represent the equilibrium adsorption capacity and the adsorption capacity at time t (min), respectively. The q_{e1} (mg/g) and k_1 (L/min) are the theoretical adsorption capacity and the rate constant, respectively.

The pseudo-second-order model can be written as:

$$t/q_t = 1/k_2 q_{e2}^2 + t/q_{e2} \quad (5)$$

where q_{e2} (mg/g) and q_t (mg/g) represent the theoretical adsorption capacity and the adsorption capacity at time t (min), respectively. k_2 (g/mg min) is the rate constant.

The Arrhenius equation was used to calculate the activation energy (E_a) of the adsorption [23]. E_a can be calculated using the following equation:

$$\ln k_2 = \ln A - (E_a/RT) \quad (6)$$

where E_a (kJ/mol) is the Arrhenius activation energy of adsorption and A is the Arrhenius factor.

The intraparticle diffusion model can be used to further analyze the process of dye adsorption onto the adsorbent, including the instantaneous adsorption phase, the gradual adsorption phase, and the final adsorption phase [24]. It can be described using the following equation:

$$q_t = K_i t^{0.5} + C_i \quad (7)$$

where q_t (mg/g) is the adsorption capacity at time t (min), the slope, K_i, and intercept, C_i, can be obtained from the straight line in the plot of q_t vs. $t^{0.5}$. K_i [mg/(g/h)] is the intraparticle diffusion constant.

2.5.2. Isotherm models

For the isotherm studies, the non-linear Langmuir isotherm, the Freundlich isotherm and the Sips isotherm were used to describe the adsorption process [25,26]. The isotherm models are described by the following equations:

$$q_e = q_m K_a C_e/(1 + K_a C_e) \quad (8)$$

$$q_e = k_f C_e^{1/n_f} \quad (9)$$

$$q_e = q_m K_s C_e^{1/n}/(1 + K_s C_e^{1/n}) \quad (10)$$

where q_m (mg/g) is the maximum adsorption capacity, K_a (L/mg) is the Langmuir adsorption constant. k_f [$mg^{1-(1/n)}/(g\ L^{-1/n})$] is the Freundlich constant and n_f is the heterogeneity factor. K_s (L/mg) is the Sips constant and n is the Sips model exponent.

2.5.3. Thermodynamic parameters

Thermodynamic parameters were used to describe whether the adsorption process is spontaneous or not, endothermic or not, and whether the absorption is favored or not [27]. The thermodynamic parameters, standard enthalpy change (ΔH°), standard entropy

change (ΔS°), and standard Gibbs free energy change (ΔG°), can be calculated using the following equations:

$$\Delta G^\circ = -RT \ln K_d \quad (11)$$

$$K_d = q_e/C_e \quad (12)$$

$$\ln K_d = -\Delta H^\circ/RT + \Delta S^\circ/R \quad (13)$$

where R is the universal gas constant (8.314 J/K mol), and K_d is the equilibrium constant for the adsorption at standard temperature and pressure.

3. Results and discussion

3.1. Characterization of the adsorbent

The FTIR spectra of MCC and MMCC are shown in Fig. 3. For MCC, the band at 3,333 cm^{-1} was attributed to the O–H stretching vibration of the hydroxyl groups in cellulose. The peak at 2,873 cm^{-1} corresponded to the C–H stretching vibration of the $–CH_2–$ groups [28]. The band at 1,642 cm^{-1} was assigned to the aldehyde carbonyl group of the terminal anhydroglucose unit. The band at 1,317 cm^{-1} was assigned to the C–O stretching vibration of the CH_2–OH groups. A series of peaks at 1,029, 1,051, 1,107, and 1,160 cm^{-1} corresponded to the –C–O–C– bonds in the anhydroglucose unit of the cellulose molecule. In the spectrum of MMCC, the peak at 3,333 cm^{-1} shifted to 3,343 cm^{-1} and became weaker. The band at 2,873 cm^{-1} became stronger and was observed as a broad shoulder peak, which indicates that new $–CH_2–$ groups had been introduced into the structure of MCC. A new absorption peak associated with the stretching vibration of a C–N bond at 1,459 cm^{-1} [29] was also observed, indicating that the quaternary ammonium group had been successfully linked to the MCC skeleton using epichlorohydrin as a bridging reagent. The band at 1,642 cm^{-1} was significantly strengthened, further demonstrating the presence of additional terminal anhydroglucose units. This shows that treatment with NaOH prior to the chemical modification made the cellulose swell in addition to causing chain breaks in the cellulose molecule.

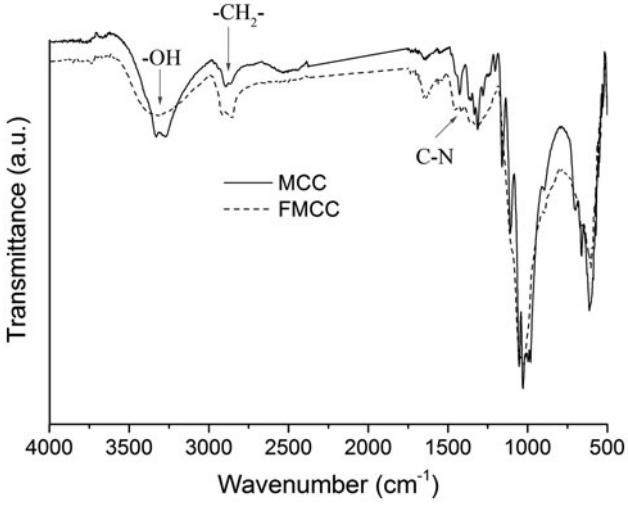

Fig. 3. FTIR spectra of MCC and MMCC.

The ^{13}C solid-state NMR spectrum of MMCC is shown in Fig. 4. The peaks were assigned using the quaternary ammonium derivatives of pectin [30], starch [31], and cellulose [32] as references. Signals 1–6 were attributed to the six carbon (C_1–C_6) atoms of the glucose unit of cellulose [33]. These exhibited lower chemical shifts than those of unmodified cellulose, representing a less-crystalline or amorphous carbon environment [14]. The lower field peak (97.92 ppm) was assigned to C_1, which was bonded to two oxygen atoms. The peak at 76.11 ppm was assigned to C_4. The peaks with chemical shifts between 69.01 and 65.31 ppm were attributed to C_2, C_3, and C_5; these overlap the peak attributed to C_7. Carbon atoms adjacent to the ether linkage bearing the cationic group (C_6') exhibited a signal of around 55.47 ppm and overlapped with peaks attributed to C_9–C_{11}. The peaks with chemical shifts between 47.82 and 44.29 ppm were attributed to C_8, C_6 (un-quaternized), and C_{10} (typical of $(CH_3)_2N^+$–). The peaks between 6.64 and 23.01 ppm were assigned to C_{12}–C_{22}. The NMR spectrum thus further confirmed successful synthesis of quaternized cellulose.

SEM photographs of MCC and MMCC, were obtained at 20,000× magnification. MCC has a smooth and compact surface structure (Fig. 5(a)). Modification visibly alters the surface, and that of MMCC (Fig. 5(b)), is much coarser, favoring the adsorption process.

3.2. The effects of adsorbent loading

The effects of MMCC dosage on the adsorption capacity for RB21 dye are shown in Fig. 6(a). The adsorption capacity decreased sharply as the MMCC dosage increased. This decrease indicates that the MMCC was not fully utilized and that a higher number of adsorption sites remained unoccupied with increased MMCC dosage [20]. The percentage removal of RB21 dye, however, increased rapidly with increased MMCC dosage and reached almost 100% when the MMCC loading was 300 mg/L at 323 K (Fig. 6(b)).

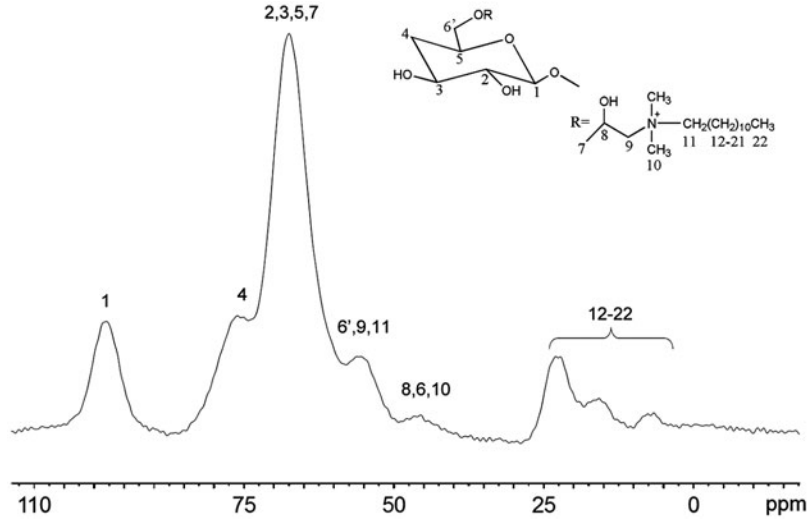

Fig. 4. ^{13}C solid-state NMR (400 MHz) spectrum of MMCC.

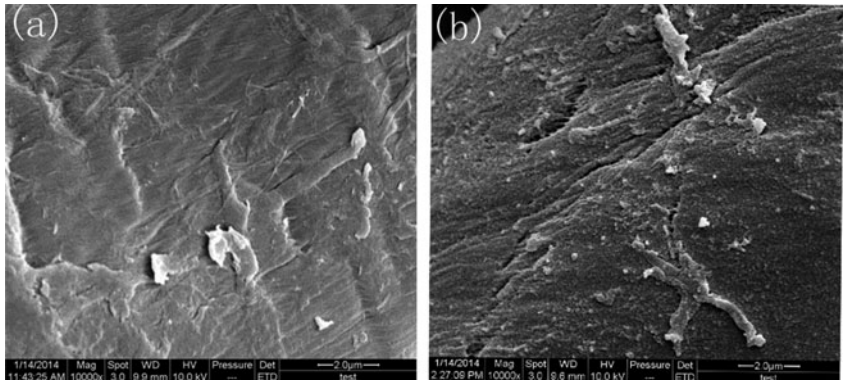

Fig. 5. SEM micrographs of MCC (a) and MMCC (b).

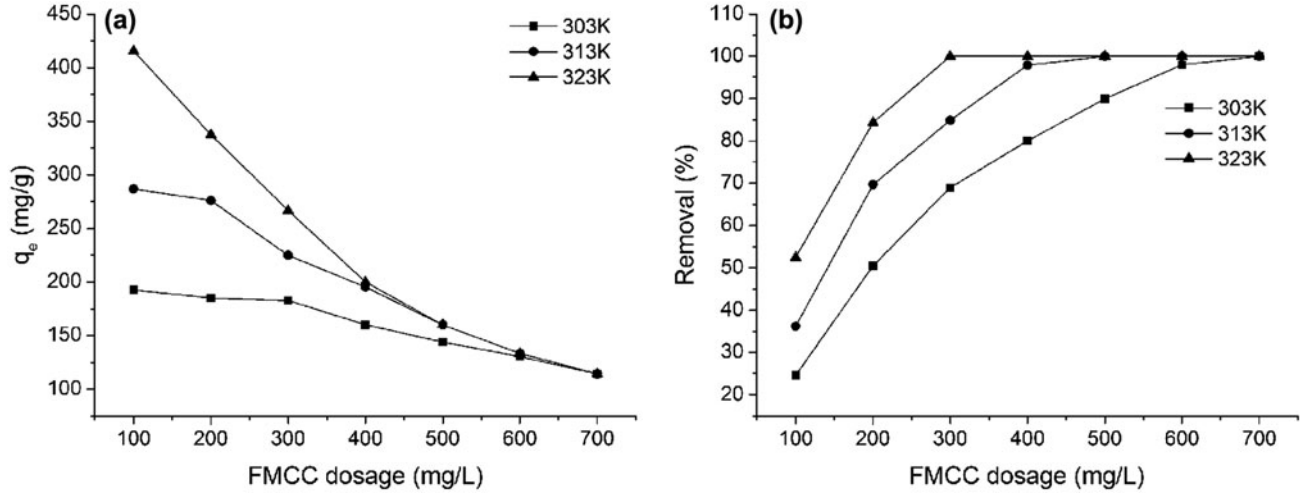

Fig. 6. Effect of MMCC dosage on the adsorption (a) and (b) of the RB21 dye (initial pH, t = 10 h, C = 80 mg/L, and V = 100 mL).

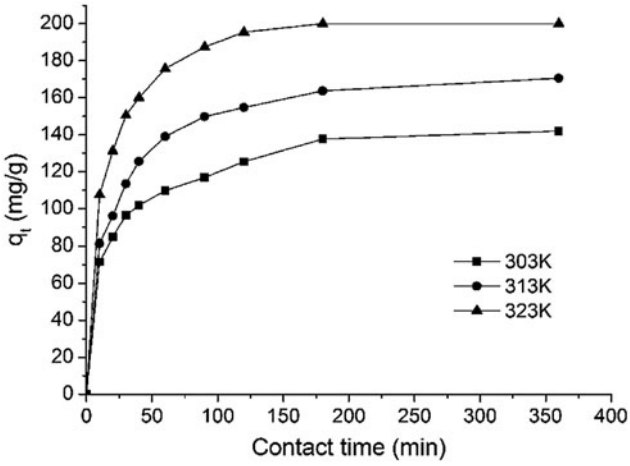

Fig. 7. Effect of contact time on the adsorption of the RB21 dye (initial pH, dosage 40 mg, C = 80 mg/L, and V = 100 mL).

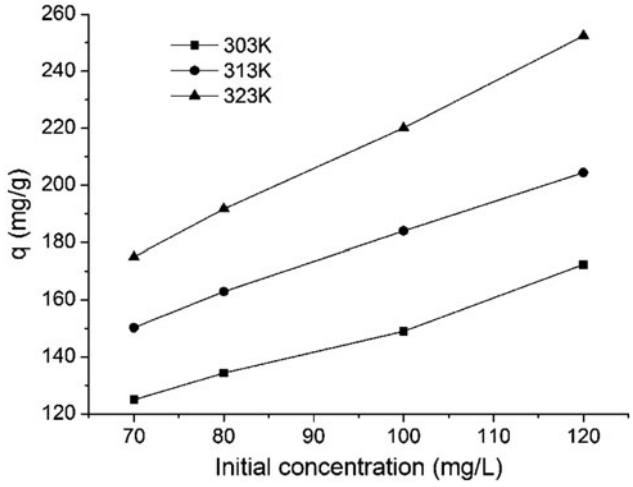

Fig. 8. Effect of initial concentration on the adsorption of the RB21 dye (initial pH, dosage 40 mg, t = 3 h, and V = 100 mL).

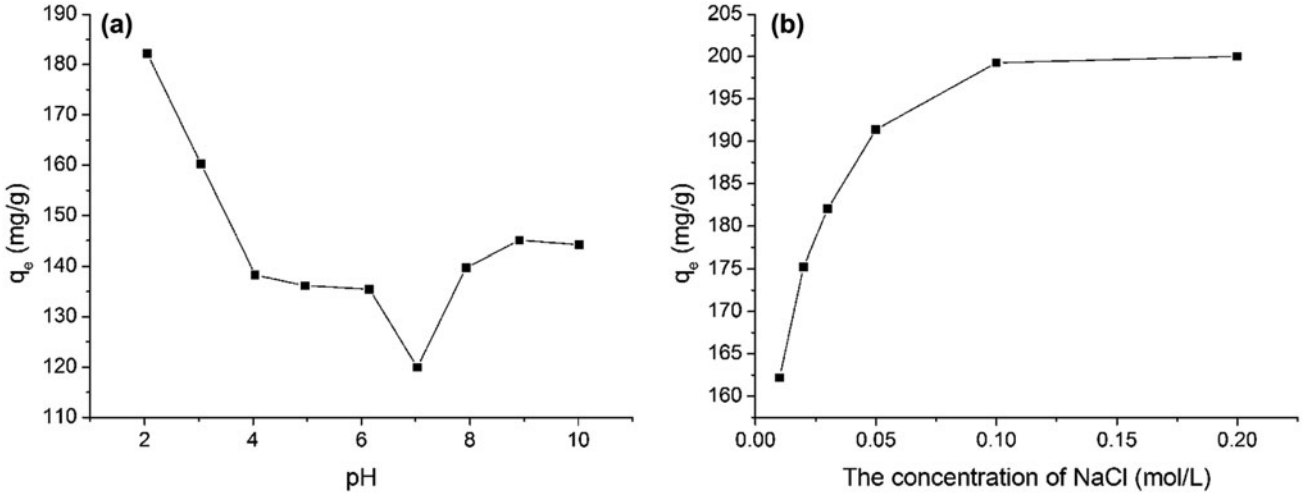

Fig. 9. Effect of solution pH values (a) and ionic strength (b) on the adsorption of the RB21 dye (dosage 40 mg, t = 3 h, T = 303 K, C = 80 mg/L, and V = 100 mL).

3.3. The effects of contact time

The effects of contact time on the adsorption of RB21 dye onto MMCC at different temperatures are shown in Fig. 7. Adsorption initially increased rapidly, and then increased more slowly to gradually reach equilibrium. Higher temperatures were found to reduce the time taken to reach equilibrium; equilibrium was reached after 180, 180, and 120 min at temperatures of 303, 313, and 323 K, respectively. Thus, 180 min was selected for next experiments.

3.4. The effects of the initial dye concentration

The influence of dye concentration on adsorption at different temperatures is depicted in Fig. 8. The adsorption capacity increased at higher concentrations of dye because of an increase in the driving force resulting from the increase in dye concentration [34]. The adsorption capacity of MMCC increased from 125.00 to 172.41 mg/g at 303 K, from 150.27 to 204.42 mg/g at 313 K, and from 175.00 to 252.41 mg/g at 323 K. This experiment also clearly illustrates that

increased temperature favors adsorption of RB21 dye onto the MMCC adsorbent. The trend towards greater adsorption capacity seen here also indicates that the MMCC adsorbent did not reach saturation under the experimental conditions [35].

3.5. The effects of pH

The pH values play a significant role in the adsorption of dyes, since the surface charges on the adsorbent, the degree of ionization, and the number of active sites are all pH-dependent [36]. Variations in equilibrium RB21 dye uptake with initial pH values in the range 2–10 are shown in Fig. 9(a). Adsorption capacity was at a minimum with an initial pH value ~7; the adsorption capacity decreased from 182.15 to 123.25 mg/g when the initial pH was increased from 2 to 7, but increased from 123.25 to 144.20 mg/g when the initial pH was increased from 7 to 10. Similar dependency of adsorption on initial pH has been found in other studies [37]. The pH_{pzc} of the MMCC adsorbent is 7.68. In theory, the adsorption capacity should reach a maximum at pH 7.68 if the electrostatic interaction is the only driving force for RB21 dye adsorption. Since adsorption did not peak at pH 7.68, other factors must be affecting the adsorption process. One of these factors is likely to be the structure of the RB21 molecule, which incorporates a sulfonic acid group ($–SO_3^-$) and a vinyl sulfone sulfate group ($–SO_2CH_2CH_2OSO_3^-$). Under strongly acidic conditions, the $–SO_3H$ groups can react with the quaternary ammonium groups on MMCC to form $–R\text{-}N^+(CH_3)_2(CH_2)_{11}SO_3^-$, which promotes adsorption of the RB21 dye. As the pH increases, the number of free $–SO_3H$ groups is reduced, resulting in fewer interactions between dye molecules and the MMCC and a decrease in adsorption capacity. RB21 dye is also

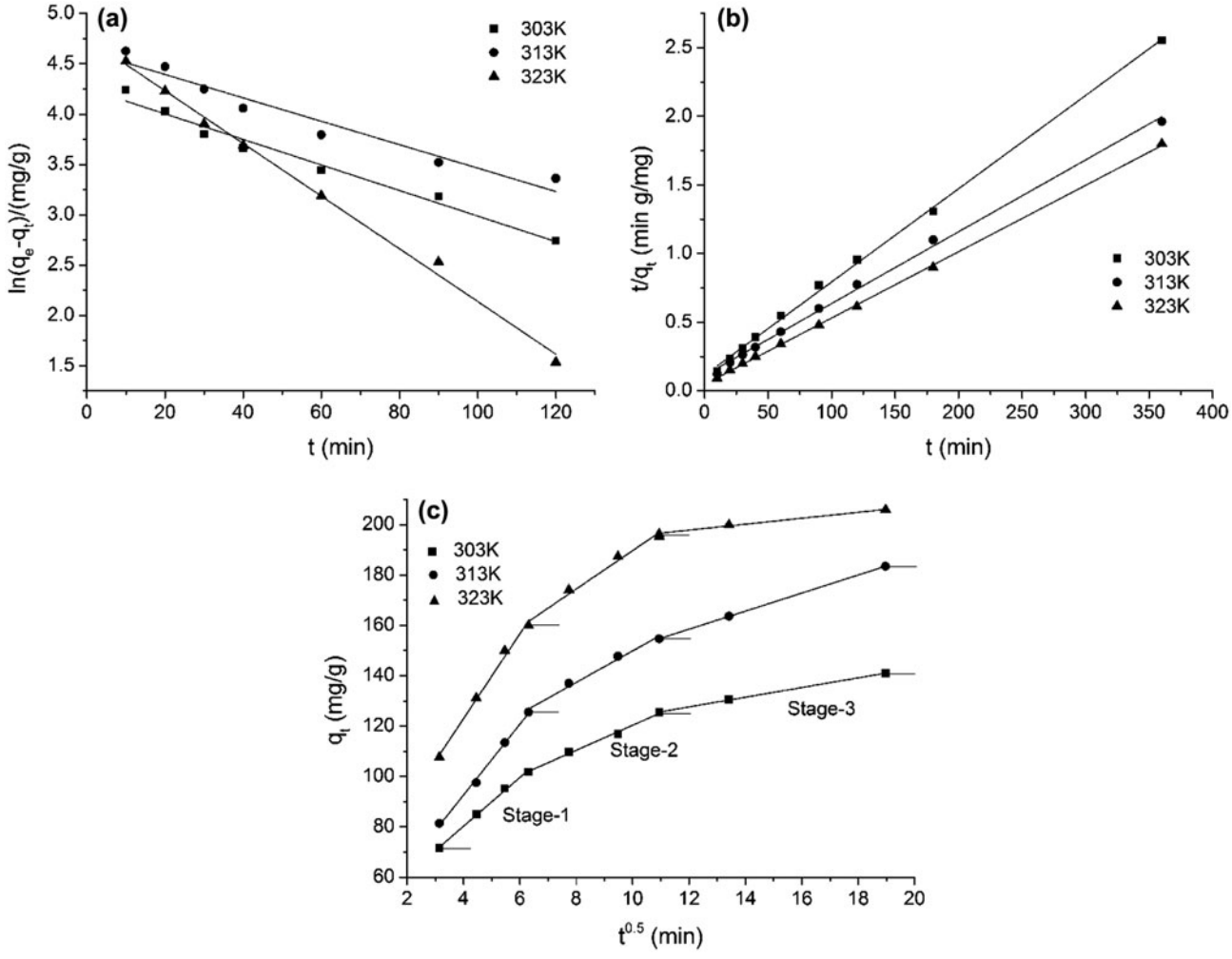

Fig. 10. Kinetics models of (a) pseudo-first-order, (b) pseudo-second-order, and (c) the intraparticle diffusion.

sensitive to high pH so that a small proportion of the vinyl sulfone sulfate groups in the molecules are converted into reactive vinyl sulfone groups under alkaline conditions. The reactive vinyl sulfone groups can then bond with unmodified hydroxyl groups in cellulose molecules, increasing the dye adsorption capacity. Higher pH values also result in dye molecule aggregation, which is favorable to the adsorption process. Overall, the adsorption capacity at alkaline pH is lower than the adsorption capacity at acidic pH. Another factor affecting adsorption is the electrostatic interaction between the dye and the adsorbent. At alkaline pH, electrostatic repulsion between the anionic dye and the negatively charged adsorbent surfaces is increased. Competition between excess OH^- ions and dye anions for adsorption sites also takes place. Our results indicate that other adsorption mechanisms, besides the electrostatic interaction, play important roles and that lower pH values favor adsorption of RB21 dye onto MMCC.

3.6. The effects of ionic strength

The effect of ionic strength on dye adsorption is illustrated in Fig. 9(b). Adsorption capacity increased from 162.18 to 200 mg/g when the NaCl concentration was increased from 0.01 to 0.2 M. Although an increase in ionic strength will generally decrease adsorption capacity due to electrostatic screening, our results did not follow this pattern. RB21 dye is so sensitive to high NaCl concentrations that aggregation of dye molecules by the salting-out effect improved adsorption onto the adsorbent [38]. The salting-out effect causes a decrease in dye solubility and a weakening of dye hydrophilicity, which results in increased adsorption of RB21 dye by the hydrophobic effect. Higher ionic strength thus improves the dye adsorption capacity of MMCC.

3.7. Adsorption kinetics

Pseudo-first-order and pseudo-second-order models have been established to evaluate the adsorption kinetics of RB21 on MMCC. The plots and parameters are summarized in Fig. 10 and Table 1. The correlation coefficients (R^2) of the pseudo-second-order model were all higher than those of the pseudo-first-order model and the calculated values of q_e from the pseudo-second-order model were closer to experimental values of q_e. These results indicate that the adsorption kinetics fit the pseudo-second-order model better than the pseudo-first-order model. The positive value of E_a was 20.16 kJ/mol, which is lower than the 40 kJ/mol threshold, indicating that adsorption of RB21 onto MMCC is a feasible physical process [39]. The intraparticle diffusion plots and parameters are shown in Fig. 10(c) and Table 1. The plots did not pass through the origin, and there were three linear portions in the plots shown as stage-1, stage-2, and stage-3. The three linear portions in the plots suggest that three steps occur in the adsorption of RB21 onto

Table 1
Kinetic parameters for RB21 dye adsorption onto MMCC

	303 K	313 K	323 K
q_e experimental (mg/g)	140.98	183.53	200.00
Pseudo-first-order model			
k_1 (1/min)	0.013	0.012	0.026
q_e calculated (mg/g)	70.57	102.17	116.25
R^2	0.975	0.939	0.995
Pseudo-second-order model			
k_2 [g/(mg min)]	6.4×10^{-4}	4.0×10^{-4}	3.9×10^{-4}
q_e calculated (mg/g)	134.77	172.71	213.22
R^2	0.997	0.998	0.999
The intraparticle diffusion			
Stage-1			
k_i [mg/(g $min^{1/2}$)]	9.72	14.11	16.89
R^2	0.996	0.997	0.999
Stage-2			
k_i [mg/(g $min^{1/2}$)]	4.97	6.27	7.63
R^2	0.993	0.983	0.979
Stage-3			
k_i [mg/(g $min^{1/2}$)]	1.92	3.59	1.18
R^2	0.998	0.999	0.988

Table 2
The parameters of adsorption isotherms for RB21 dye onto MMCC

	Temperature		
The parameters	303 K	308 K	313 K
Freundlich model			
$1/n_f$	0.19	0.15	0.13
k_f [$mg^{1-(1/n)}$/(g $L^{-1/n}$)]	111.70	175.95	208.04
R^2	0.856	0.878	0.863
Langmuir model			
q_m (mg/g)	191.95	273.50	408.90
K_a (L/mg)	0.58	0.75	0.84
R^2	0.996	0.990	0.991
Sips model			
q_m (mg/g)	256.41	337.57	547.29
K_s	0.36	0.43	0.67
$1/n$	0.88	0.76	0.40
R^2	0.972	0.967	0.976
q_e (mg/g)	140.98	183.53	200.00

Table 3
Comparison of maximum adsorption capacity (q_{max}) of various adsorbents for RB21 dye

Adsorbents	Adsorption isotherm	Temperature, T (K)	q_{max} (mg/g)	Reference
Quaternized MCC	Langmuir	313	408.90	This work
Fly ash	Langmuir	323	106.71	[43]
Powdered activated carbon	Langmuir	298	101.00	[44]
Dried *Rhizopus arrhizus*	Langmuir	308	92.20	[45]
Sugar beet pulp	Langmuir	313	83.70	[46]
Sepiolite	Langmuir	323	66.67	[43]
Carbonized beet pulp	Langmuir	298	52.63	[47]
Immobilized scendesmus	Langmuir	303	45.70	[48]

MMCC: the instantaneous adsorption process, the gradual adsorption process, and the final adsorption process [40]. Stage-1 was attributed to adsorption of RB21 onto the adsorbent surface and was the fastest process. In stage-2, the adsorption rate started to slow down because of the dominant effect of intraparticle diffusion. In stage-3, leading to equilibrium adsorption, the adsorption rate was the slowest because of the decreasing dye concentration in the solution. These data suggest that intraparticle diffusion is the rate-limiting step in the dye adsorption process [41].

3.8. Adsorption isotherms

The non-linear forms of Langmuir, Freundlich, and Sips isotherms were used to evaluate the adsorption properties of the adsorbent. The calculated parameters from the Langmuir and Freundlich adsorption models for RB21 dye onto MMCC are shown in Table 2. Comparing correlation coefficients (R^2), the Langmuir model best describes the adsorption process of RB21 dye onto MMCC, suggesting a monolayer adsorption process, without interaction between the adsorbed dye molecules [42]. The values of Ka were in the range 0–1, which favors adsorption of RB21 dye onto MMCC. Consistent with the result of the Langmuir model, the value of $1/n$ obtained from the Freundlich model < 1, which also suggests that adsorption of RB21 dye onto MMCC is favorable. Compared with the maximum adsorption capacities for RB21 dye of other materials (Table 3), the maximum adsorption capacity for RB21 dye on MMCC is much higher, showing that MMCC is highly efficient for removing RB21 dye from aqueous solutions.

3.9. Adsorption thermodynamics

Thermodynamic parameters (Table 4) were determined by studying the adsorption of RB21 dye onto MMCC at different temperatures. The negative value of ΔG° decreased with increasing temperature, indicating that adsorption of RB21 dye onto MMCC is spontaneous and feasible. The ΔH° value of 69.00 kJ/mol is in the range 20–80 kJ/mol, indicating that the adsorption is a physical interaction between dye molecules and adsorbent [43]. The positive ΔH° value indicates that the adsorption is an endothermic process and that increased temperatures will favor adsorption. The positive value of ΔS° indicates that randomness increases at the interface during the adsorption process.

Table 4
Thermodynamic parameters for adsorption of RB21 dye onto MMCC

		ΔG° (kJ/mol)		
ΔH° (kJ/mol)	ΔS° [J/(mol K)]	303 K	308 K	313 K
69.00	241.19	−4.11	−6.33	−8.84

4. Conclusions

Removal of RB21 dye from aqueous solutions was studied using a new chemically MMCC with attached hydroxypropyldodecyldimethylammonium groups. Spectral and microscopic characterization proved that the quaternary ammonium group had been successfully attached to the cellulose and that the surface of the modified material was coarser than that of MCC. Lower initial pH values and higher temperatures of the dye solution were favorable to the adsorption. The adsorption capacity reached 200 mg/g at the initial pH at a loading of 400 mg/L and an initial concentration of 80 mg/L. The kinetics of the adsorption conformed well to the pseudo-second-order model and the adsorption isotherm was consistent with the Langmuir model. Thermodynamic studies indicated that

the adsorption of RB21 dye onto MMCC is a spontaneous endothermic process. The study indicates that MMCC may be effective in removing anionic dyes from wastewater.

Acknowledgments

The authors gratefully acknowledge the support from the Fundamental Research Funds of the Central Universities (2572015AB05).

References

[1] E.S. Abdel-Halim, S.S. Al-Deyab, Removal of heavy metals from their aqueous solutions through adsorption onto natural polymers, Carbohydr. Polym. 84 (2011) 454–458.
[2] M.A.M. Salleh, D.K. Mahmoud, W.A.W.A. Karim, A. Idris, Cationic and anionic dye adsorption by agricultural solid wastes: A comprehensive review, Desalination 280 (2011) 1–13.
[3] J.L. Gong, B. Wang, G.M. Zeng, C.P. Yang, C.G. Niu, Q.Y. Niu, W.J. Zhou, Y. Liang, Removal of cationic dyes from aqueous solution using magnetic multi-wall carbon nanotube nanocomposite as adsorbent, J. Hazard. Mater. 164 (2009) 1517–1522.
[4] G. Bayramoglu, M. Yakuparica, Adsorption of Cr(VI) onto PEI immobilized acrylate-based magnetic beads: Isotherms, kinetics and thermodynamics study, Chem. Eng. J. 139 (2008) 20–28.
[5] T. Liu, Y. Li, Q. Du, J. Sun, Y. Jiao, G. Yang, Z. Wang, Y. Xia, W. Zhang, K. Wang, H. Zhu, D. Wu, Adsorption of methylene blue from aqueous solution by graphene, Colloids Surf., B 90 (2012) 197–203.
[6] Z. Aksu, I.A. Isoglu, Use of agricultural waste sugar beet pulp for the removal of Gemazol turquoise blue-G reactive dye from aqueous solution, J. Hazard. Mater. 137 (2006) 418–430.
[7] S. Sekar, M. Surianarayanan, V. Ranganathan, D.R. MacFarlane, A.B. Mandal, Choline-based ionic liquids-enhanced biodegradation of azo dyes, Environ. Sci. Technol. 46 (2012) 4902–4908.
[8] D. Pokhrel, T. Viraraghavan, Treatment of pulp and paper mill wastewater—A review, Sci. Total Environ. 333 (2004) 37–58.
[9] S. Chakraborty, S. De, S. DasGupta, J.K. Basu, Adsorption study for the removal of a basic dye: Experimental and modeling, Chemosphere 58 (2005) 1079–1086.
[10] G.G. Stavropoulos, P. Samaras, G.P. Sakellaropoulos, Effect of activated carbons modification on porosity, surface structure and phenol adsorption, J. Hazard. Mater. 151 (2008) 414–421.
[11] C.-H. Zhou, D. Zhang, D.-S. Tong, L.-M. Wu, W.-H. Yu, S. Ismadji, Paper-like composites of cellulose acetate–organo-montmorillonite for removal of hazardous anionic dye in water, Chem. Eng. J. 209 (2012) 223–234.
[12] D. Klemm, B. Heublein, H.P. Fink, A. Bohn, Cellulose: Fascinating biopolymer and sustainable raw material, Angew. Chem. Int. Ed. 44 (2005) 3358–3393.
[13] X. Guo, Y. Du, F. Chen, H.S. Park, Y. Xie, Mechanism of removal of arsenic by bead cellulose loaded with iron oxyhydroxide (β-FeOOH): EXAFS study, J. Colloid Interface Sci. 314 (2007) 427–433.
[14] L.S. Silva, L.C.B. Lima, F.C. Silva, J.M.E. Matos, M.R.M.C. Santos, L.S. Santos Júnior, K.S. Sousa, E.C. da Silva Filho, Dye anionic sorption in aqueous solution onto a cellulose surface chemically modified with aminoethanethiol, Chem. Eng. J. 218 (2013) 89–98.
[15] W. Shen, S.Y. Chen, S.K. Shi, X. Li, X. Zhang, W.L. Hu, H.P. Wang, Adsorption of Cu(II) and Pb(II) onto diethylenetriamine-bacterial cellulose, Carbohydr. Polym. 75 (2009) 110–114.
[16] G. Ronca, L. Palmieri, S. Maltinti, D. Tagliazucchi, A. Conte, Relationship between iron and protein content of dishes and polyphenol content in accompanying wines, Drug Exp. Clin. Res. 29 (2003) 271–286.
[17] R.M. El-Shishtawy, A. Hashem, Preparation and characterization of cationized cellulose for the removal of anionic dyes, Adsorpt. Sci. Technol. 19 (2001) 197–210.
[18] W. Zhang, H. Li, X. Kan, L. Dong, H. Yan, Z. Jiang, H. Yang, A. Li, R. Cheng, Adsorption of anionic dyes from aqueous solutions using chemically modified straw, Bioresour. Technol. 117 (2012) 40–47.
[19] X.Y. Zhang, J. Tan, X.H. Wei, L.J. Wang, Removal of Remazol turquoise Blue G-133 from aqueous solution using modified waste newspaper fiber, Carbohydr. Polym. 92 (2013) 1497–1502.
[20] Y. Qi, J. Li, L.J. Wang, Removal of Remazol Turquoise Blue G-133 from aqueous medium using functionalized cellulose from recycled newspaper fiber, Ind. Crops Prod. 50 (2013) 15–22.
[21] A.K. Verma, R.R. Dash, P. Bhunia, A review on chemical coagulation/flocculation technologies for removal of colour from textile wastewaters, J. Environ. Manage. 93 (2012) 154–168.
[22] Y.S. Ho, G. McKay, Sorption of dye from aqueous solution by peat, Chem. Eng. J. 70 (1998) 115–124.
[23] L. Wang, J. Li, Adsorption of C.I. Reactive Red 228 dye from aqueous solution by modified cellulose from flax shive: Kinetics, equilibrium, and thermodynamics, Ind. Crops Prod. 42 (2013) 153–158.
[24] Y.S. Ho, Review of second-order models for adsorption systems, J. Hazard. Mater. 136 (2006) 681–689.
[25] K.V. Kumar, S. Sivanesan, Prediction of optimum sorption isotherm: Comparison of linear and non-linear method, J. Hazard. Mater. 126 (2005) 198–201.
[26] M. Sprynskyy, T. Kowalkowski, H. Tutu, E.M. Cukrowska, B. Buszewski, Ionic liquid modified diatomite as a new effective adsorbent for uranium ions removal from aqueous solution, Colloids Surf., A 465 (2015) 159–167.
[27] W. Cheah, S. Hosseini, M.A. Khan, T.G. Chuah, T.S.Y. Choong, Acid modified carbon coated monolith for methyl orange adsorption, Chem. Eng. J. 215–216 (2013) 747–754.
[28] A.M. Adel, Z.H. Abd El-Wahab, A.A. Ibrahim, M.T. Al-Shemy, Characterization of microcrystalline cellulose prepared from lignocellulosic materials. Part II: Physicochemical properties, Carbohydr. Polym. 83 (2011) 676–687.
[29] W. Cao, Z. Dang, X.Q. Zhou, X.Y. Yi, P.X. Wu, N.W. Zhu, G.N. Lu, Removal of sulphate from aqueous solution using modified rice straw: Preparation,

characterization and adsorption performance, Carbohydr. Polym. 85 (2011) 571–577.
[30] L.H. Fan, M. Cao, S. Gao, W.P. Wang, K. Peng, C. Tan, F. Wen, S.X. Tao, W.G. Xie, Preparation and characterization of a quaternary ammonium derivative of pectin, Carbohydr. Polym. 88 (2012) 707–712.
[31] Y.X. Jiang, B.Z. Ju, S.F. Zhang, J.Z. Yang, Preparation and application of a new cationic starch ether—Starch–methylene dimethylamine hydrochloride, Carbohydr. Polym. 80 (2010) 467–473.
[32] Y. Song, J. Zhang, W. Gan, J. Zhou, L. Zhang, Flocculation properties and antimicrobial activities of quaternized celluloses synthesized in NaOH/urea aqueous solution, Ind. Eng. Chem. Res. 49 (2010) 1242–1246.
[33] B. Belhalfaoui, A. Aziz, El Hadj Elandaloussi, M.S. Ouali, L.C. De Ménorval, Succinate-bonded cellulose: A regenerable and powerful sorbent for cadmium-removal from spiked high-hardness groundwater, J. Hazard. Mater. 169 (2009) 831–837.
[34] M.-S. Chiou, H.-Y. Li, Equilibrium and kinetic modeling of adsorption of reactive dye on cross-linked chitosan beads, J. Hazard. Mater. 93 (2002) 233–248.
[35] M.H. Min, L.D. Shen, G.S. Hong, M.F. Zhu, Y. Zhang, X.F. Wang, Y.M. Chen, B.S. Hsiao, Micro-nano structure poly(ether sulfones)/poly(ethyleneimine) nanofibrous affinity membranes for adsorption of anionic dyes and heavy metal ions in aqueous solution, Chem. Eng. J. 197 (2012) 88–100.
[36] S.A. Ong, L.N. Ho, Y.S. Wong, A. Zainuddin, Adsorption behavior of cationic and anionic dyes onto acid treated coconut coir, Sep. Sci. Technol. 48 (2013) 2125–2131.
[37] S. Rosa, M.C. Laranjeira, H.G. Riela, V.T. Fávere, Cross-linked quaternary chitosan as an adsorbent for the removal of the reactive dye from aqueous solutions, J. Hazard. Mater. 155 (2008) 253–260.
[38] C. Shuang, P. Li, A. Li, Q. Zhou, M. Zhang, Y. Zhou, Quaternized magnetic microspheres for the efficient removal of reactive dyes, Water Res. 46 (2012) 4417–4426.
[39] W. Konicki, D. Sibera, E. Mijowska, Z. Lendzion-Bieluń, U. Narkiewicz, Equilibrium and kinetic studies on acid dye Acid Red 88 adsorption by magnetic $ZnFe_2O_4$ spinel ferrite nanoparticles, J. Colloid Interface Sci. 398 (2013) 152–160.
[40] X.Y. Huang, J.-P. Bin, H.-T. Bu, G.-B. Jiang, M.-H. Zeng, Removal of anionic dye eosin Y from aqueous solution using ethylenediamine modified chitosan, Carbohydr. Polym. 84 (2011) 1350–1356.
[41] J. Wang, L. Xu, Y. Meng, C. Cheng, A. Li, Adsorption of Cu^{2+} on new hyper-crosslinked polystyrene adsorbent: Batch and column studies, Chem. Eng. J. 178 (2011) 108–114.
[42] L. Zhou, J. Huang, B. He, F. Zhang, H. Li, Peach gum for efficient removal of methylene blue and methyl violet dyes from aqueous solution, Carbohydr. Polym. 101 (2014) 574–581.
[43] E. Demirbas, M.Z. Nas, Batch kinetic and equilibrium studies of adsorption of Reactive Blue 21 by fly ash and sepiolite, Desalination 243 (2009) 8–21.
[44] F. Kargi, S. Ozmıhcı, Comparison of adsorption performances of powdered activated sludge and powdered activated carbon for removal of turquoise blue dyestuff, Process Biochem. 40 (2005) 2539–2544.
[45] Z. Aksu, S.S. Çağatay, Investigation of biosorption of Gemazol Turquise Blue-G reactive dye by dried *Rhizopus arrhizus* in batch and continuous systems, Sep. Purif. Technol. 48 (2006) 24–35.
[46] Z. Aksu, I.A. Isoglu, Use of agricultural waste sugar beet pulp for the removal of Gemazol turquoise blue-G reactive dye from aqueous solution, J. Hazard. Mater. 137 (2006) 418–430.
[47] A.Y. Dursun, O. Tepe, G. Dursun, Use of carbonised beet pulp carbon for removal of Remazol Turquoise Blue-G 133 from aqueous solution, Environ. Sci. Pollut. Res. Int. 20 (2013) 431–442.
[48] A. Ergene, K. Ada, S. Tan, H. Katırcıoğlu, Removal of Remazol Brilliant Blue R dye from aqueous solutions by adsorption onto immobilized Scenedesmus quadricauda: Equilibrium and kinetic modeling studies, Desalination 249 (2009) 1308–1314.